Published in final edited form as:
Angiogenesis. 2013 July ; 16(3): 663–674. doi:10.1007/s10456-013-9344-y.

Imaging tumor angiogenesis in breast cancer experimental lung metastasis with positron emission tomography, near-infrared fluorescence, and bioluminescence

Yin Zhang[1], **Hao Hong**[2], **Tapas R. Nayak**[2], **Hector F. Valdovinos**[1], **Duane V. Myklejord**[2], **Charles P. Theuer**[3], **Todd E. Barnhart**[1], and **Weibo Cai**[1,2,4,*]

[1]Department of Medical Physics, University of Wisconsin - Madison, Madison, WI, USA

[2]Department of Radiology, University of Wisconsin - Madison, Madison, WI, USA

[3]TRACON Pharmaceuticals, Inc., San Diego, CA, USA

[4]University of Wisconsin Carbone Cancer Center, Madison, WI, USA

Abstract

The goal of this study was to develop a molecular imaging agent that can allow for both positron emission tomography (PET) and near-infrared fluorescence (NIRF) imaging of CD105 expression in metastatic breast cancer. TRC105, a chimeric anti-CD105 monoclonal antibody, was labeled with both a NIRF dye (i.e., IRDye 800CW) and ^{64}Cu to yield ^{64}Cu-NOTA-TRC105-800CW. Flow cytometry analysis revealed no difference in CD105 binding affinity/specificity between TRC105 and NOTA-TRC105-800CW. Serial bioluminescence imaging (BLI) was carried out to non-invasively monitor the lung tumor burden in BALB/c mice, after intravenous injection of firefly luciferase-transfected 4T1 (i.e., fLuc-4T1) murine breast cancer cells to establish the experimental lung metastasis model. Serial PET imaging revealed that fLuc-4T1 lung tumor uptake of ^{64}Cu-NOTA-TRC105-800CW was 11.9 ± 1.2, 13.9 ± 3.9, and 13.4 ± 2.1 %ID/g at 4, 24, and 48 h post-injection respectively (n = 3). Biodistribution studies, blocking fLuc-4T1 lung tumor uptake with excess TRC105, control experiments with ^{64}Cu-NOTA-cetuximab-800CW (which served as an isotype-matched control), ex vivo BLI/PET/NIRF imaging, autoradiography, and histology all confirmed CD105 specificity of ^{64}Cu-NOTA-TRC105-800CW. Successful PET/NIRF imaging of tumor angiogenesis (i.e., CD105 expression) in the breast cancer experimental lung metastasis model warrants further investigation and clinical translation of dual-labeled TRC105-based agents, which can potentially enable early detection of small metastases and image-guided surgery for tumor removal.

Keywords

Breast cancer; Tumor angiogenesis; Lung metastasis; Positron emission tomography (PET); Near-infrared fluorescence (NIRF); CD105/endoglin; ImmunoPET; Image-guided surgery

Introduction

Breast cancer (BC) is the most frequently diagnosed cancer type and the second leading cause of cancer mortality among women in the United States, with estimated 226,870 new cases and 39,510 deaths in 2012 [1]. The majority of deaths in BC patients are from

Requests for reprints: Weibo Cai, PhD, Departments of Radiology and Medical Physics, University of Wisconsin - Madison, Room 7137, 1111 Highland Avenue, Madison, WI 53705, USA, wcai@uwhealth.org; Phone: 608-262-1749; Fax: 608-265-0614.

metastases instead of the primary tumors [2], and studies have shown that BC preferentially metastasizes to the lung, liver, and bones [3]. Many anatomical imaging techniques such as X-ray, computed tomography (CT), magnetic resonance imaging (MRI), and ultrasound (US) have been used in the management of metastatic BC patients. Although these techniques may be used for tumor size measurement, in many cases they cannot differentiate benign and malignant lesions. ^{18}F-FDG positron emission tomography (PET), commonly used in clinical oncology [4–6], has also been used for staging and management of BC. However, it is a general marker for glucose metabolism and may result in inflammation-related false-positive findings. There is an urgent need for new molecular imaging agents that can allow for early (metastatic) lesion detection, treatment planning, image-guided tumor removal, and effective monitoring of therapeutic responses for BC patients.

Angiogenesis plays a crucial role in the growth, invasion, and metastasis of solid tumors, which has been long recognized as a hallmark of cancer [7]. High level of tumor angiogenic activity often results in poor prognosis of BC patients. For example, expression of transforming growth factor-β (TGF-β) has been correlated with increased metastasis in BC [8, 9]. CD105 (also called endoglin), a 180 kDa transmembrane glycoprotein primarily over-expressed on activated endothelial cells, is a co-receptor of TGF-β and plays an important role in the TGF-β signaling pathway [10, 11]. Many studies have shown that high CD105 expression correlates with poor prognosis and decreased survival in multiple solid tumor types, including metastatic BC [11]. The fact that CD105 is almost exclusively expressed on activated endothelial cells makes it an ideal marker for angiogenesis, which holds tremendous potential as a diagnostic, prognostic, and therapeutic target in both primary and metastatic BC.

PET imaging has been commonly used in clinical oncology for tumor staging and monitoring of therapeutic efficacy [4, 12, 13], which is highly sensitive (down to the picomolar level) with superb tissue penetration of signal. However, the spatial resolution of PET is comparatively low (i.e., a few mm) [14]. Optical imaging in the near-infrared (NIR, 700–900 nm) region can provide better spatial resolution and acceptable tissue penetration of signal in small animal studies and certain clinical scenarios, such as BC imaging, image-guided surgery, etc. [14, 15]. The combination of PET and NIR fluorescence (NIRF) imaging using a single molecularly targeted agent can provide complementary information and synergistic advantages that neither modality alone can offer [14, 16–18].

TRC105 is a human/murine chimeric IgG1 monoclonal antibody (mAb) that binds to both human and murine CD105 with high avidity (with a K_D of 2 ng/mL for human CD105) [19]. It has recently completed a multicenter first-in-human dose-escalation trial [20], with multiple phase 2 trials ongoing in various solid tumor types. The goal of this study was to develop a single molecular imaging agent which can allow for both PET and NIRF imaging of small nodules in BC lung metastases. TRC105 was labeled with ^{64}Cu ($t_{1/2}$: 12.7 h, β^+: 17.4%) and a NIRF dye, IRDye 800CW (Ex/Em: 778/806 nm), and the resulting tracer was investigated for PET/NIRF imaging of CD105 expression in a BC experimental lung metastasis model. Cetuximab, which only binds to human epidermal growth factor receptor (EGFR) but not murine EGFR, was used as an isotype matched control. 4T1 murine BC cells were stably transfected with firefly luciferase (denoted as fLuc-4T1) to allow for non-invasive monitoring of the tumor growth in mouse lungs with serial bioluminescence imaging (BLI). This dual-labeled imaging agent is expected to provide whole-body information on the angiogenic activity of all metastatic lesions, as well as facilitate NIRF image-guided surgery to remove the tumor nodules at an early phase.

Materials and methods

Reagents

TRC105 was provided by TRACON pharmaceuticals Inc. (San Diego, CA). Cetuximab was from Bristol-Meyers Squibb Company (Princeton, NJ). AlexaFluor488- and Cy3-labeled secondary antibodies were purchased from Jackson Immunoresearch Laboratories, Inc. (West Grove, CA). 2-S-(4-isothiocyanatobenzyl)-1,4,7-triazacyclononane-1,4,7-triacetic acid (p-SCN-Bn-NOTA; Macrocyclics, Inc., Dallas, TX), Chelex 100 resin (50–100 mesh, Sigma-Aldrich, St. Louis, MO), IRDye 800CW-NHS ester (LI-COR Biosciences Co., Lincoln, NE), D-Luciferin (Gold BioTechnology, St Louis, MO), and PD-10 desalting columns (GE Healthcare, Piscataway, NJ) were all acquired from commercial sources. Water and all buffers were of Millipore grade and pre-treated with Chelex 100 resin to ensure that the aqueous solution was heavy metal-free. All other reaction buffers and chemicals were from Thermo Fisher Scientific (Fair Lawn, NJ).

Cell lines and animal model

4T1 murine BC, MCF-7 human BC, and human umbilical vein endothelial cells (HUVECs) were purchased from the American Type Culture Collection (ATCC, Manassas, VA). Detail procedure for stable transfection of 4T1 cells with firefly luciferase has been reported previously [21]. fLuc-4T1 and MCF-7 cells were cultured in RPMI 1640 medium (Invitrogen, Carlsbad, CA) with 10% fetal bovine serum and incubated at 37 °C with 5% CO_2. HUVECs were cultured in M-200 medium (Invitrogen, Carlsbad, CA) with 1× low serum growth supplement (Cascade Biologics, Portland, OR) and incubated at 37 °C with 5% CO_2. Cells were used for in vitro and in vivo experiments when they reached ~75% confluence.

All animal studies were conducted under a protocol approved by the University of Wisconsin Institutional Animal Care and Use Committee. The fLuc-4T1 BC experimental lung metastasis model was established by intravenous (i.v.) injection of 2×10^5 fLuc-4T1 cells in 100 μL of phosphate-buffered saline (PBS) into 6-week-old female BALB/C mice (Harlan, Madison, WI) via tail vein. BLI signal of the mice was monitored regularly using an IVIS Spectrum system (PerkinElmer, Branford, CT). Mice were used for PET/NIRF imaging studies when the BLI signals from the thoracic area of mice were substantially strong (typically 3 weeks after injection).

NOTA/800CW-conjugation and ^{64}Cu-labeling

NOTA-conjugation was carried out at pH 9.0, with the ratio of p-SCN-Bn-NOTA:mAb being 25:1. NOTA-TRC105 and NOTA-cetuximab were purified using PD-10 columns with PBS as the mobile phase. After NOTA conjugation, a molar ratio of 2:1 was used for the reactions between IRDye 800CW-NHS and NOTA-TRC105 or NOTA-cetuximab. The pH value of the reaction mixtures was adjusted to 8.5 with 0.1 M Na_2CO_3. After continuously stirring the reaction mixture at room temperature (RT) for 2 h, NOTA-TRC105-800CW and NOTA-cetuximab-800CW were purified by size exclusion column chromatography.

^{64}Cu was produced via a ^{64}Ni(p,n)^{64}Cu reaction using a GE PETtrace cyclotron, with a specific activity of ~ 5 Ci/μmol at the end of bombardment. For radiolabeling, $^{64}CuCl_2$ (74 MBq) was diluted in 300 μL of 0.1 M sodium acetate buffer (pH 6.5) and added to 50 μg of NOTA-TRC105-800CW or NOTA-cetuximab-800CW. The reaction mixture was incubated for 30 min at 37 °C with constant shaking. ^{64}Cu-NOTA-TRC105-800CW and ^{64}Cu-NOTA-cetuximab-800CW were purified using PD-10 columns with PBS as the mobile phase. The radioactive fractions containing ^{64}Cu-NOTA-TRC105-800CW or ^{64}Cu-NOTA-

cetuximab-800CW were collected and passed through a 0.2 μm syringe filter for in vivo experiments.

Flow cytometry

The immunoreactivity of TRC105 and NOTA-TRC105-800CW to HUVECs (high CD105 expression) and MCF-7 cells (CD105 negative) were evaluated by fluorescence-activated cell sorting (FACS) analysis. Briefly, cells were harvested and suspended in cold PBS with 2% bovine serum albumin at a concentration of 5×10^6 cells/mL. The cells were incubated with various concentrations of TRC105 or NOTA-TRC105-800CW (1, 5, or 10 μg/mL) for 30 min at RT, and washed three times with cold PBS. The cells were then incubated with AlexaFluor488-labeled goat anti-human IgG (5 μg/mL) for 30 min at RT. Afterwards, the cells were washed and analyzed by FACS using a BD FACSCalibur 4-color analysis cytometer, which is equipped with 488 and 633nm lasers (Becton-Dickinson, San Jose, CA) and FlowJo analysis software (Tree Star, Inc., Ashland, OR).

Imaging and biodistribution studies

PET and PET/CT scans at various time points post-injection (p.i.) using an Inveon microPET/microCT rodent model scanner (Siemens Medical Solutions USA, Inc.), image reconstruction, and region-of-interest (ROI) analysis were performed similar as our previous reports [22–24]. Each fLuc-4T1 lung tumor-bearing mouse was intravenously injected with 5–10 MBq of the PET tracer (containing ~300 picomoles of conjugated IRDye 800CW) via tail vein, and 5–10 min static PET scans were carried out. Quantitative data were presented as percentage of injected dose per gram of tissue (%ID/g, mean ± SD). A cohort of three fLuc-4T1 lung tumor-bearing mice was each injected with 2 mg of TRC105 at 2 h before ^{64}Cu-NOTA-TRC105-800CW administration to evaluate the CD105 specificity of ^{64}Cu-NOTA-TRC105-800CW in vivo (i.e., blocking experiment).

BLI was carried out with an IVIS Spectrum system after intraperitoneal (i.p.) injection of D-luciferin (150 mg/kg of mouse body weight), either at ~10 minutes after injection (in vivo) or shortly after euthanasia and organ harvesting (ex vivo), while NIRF imaging was performed in the same system using an excitation filter of 745 nm (width: 30 nm) and emission filter of 800 nm (width: 20 nm).

A subset of fLuc-4T1 tumor-bearing lungs was placed on a phosphor-imaging film for high resolution autoradiography. After 30 min of exposure, the films were scanned in a Cyclone Storage Phosphor Screen System (PerkinElmer, Branford, CT). The fLuc-4T1 tumor-bearing lungs were subsequently scanned in the IVIS Spectrum system to acquire images at high resolution for comparison with the autoradiography data. Biodistribution studies were carried out after the last PET scans to validate the PET results. The fLuc-4T1 tumor-bearing lung, liver, and spleen (i.e., tissues with significant uptake of ^{64}Cu-NOTA-TRC105-800CW) were also frozen for histological analysis.

Histology

Frozen tissue slices of 5 μm thickness were fixed with cold acetone for 10 min and dried in the air for 30 min. After rinsing with PBS and blocking with 10% donkey serum for 30 min at RT, the slices were incubated with TRC105 (2 μg/mL) for 1 h at 4 °C and visualized using AlexaFluor488-labeled goat anti-human IgG. The tissue slices were also stained for endothelial marker CD31 as described previously [25, 26], using a rat anti-mouse CD31 antibody (2 μg/mL) and a Cy3-labeled donkey anti-rat IgG. Cell nuclei in the slices of fLuc-4T1 tumor-bearing lung were visualized by addition of mounting medium with 4',6-diamidino-2-phenylindole (DAPI; Vector lab, Burlingame, CA) before microscopy

examination. All images were acquired with a Nikon Eclipse Ti microscope under the same condition and displayed at the same scale. Magnification: 200×.

Statistical analysis

Quantitative data were expressed as mean ± SD. Means were compared using Student's t-test. P values < 0.05 were considered statistically significant.

Results

Synthesis and characterization of the PET/NIRF probe

In the final conjugates (NOTA-TRC105-800CW or NOTA-cetuximab-800CW), on average ~5 NOTA and ~0.9 IRDye 800CW molecules were conjugated to each mAb. Less than one 800CW per mAb will avoid any self-quenching due to close proximity of 800CW molecules, since fluorescence resonance energy transfer only occurs when two 800CW molecules are within a distance of 10 nm (about the size of an mAb). Such minimal NOTA/800CW conjugation of TRC105 did not alter its CD105 binding affinity, as evidenced by FACS analysis of HUVECs (which express a high level of CD105 [16, 17]) (Figure 1a). No observable differences were found between TRC105 and NOTA-TRC105-800CW at 1 μg/mL or 5 μg/mL concentrations, both at non-saturating conditions. On the other hand, neither TRC105 nor NOTA-TRC105-800CW bound to CD105-negative MCF-7 cells, even at a much higher concentration of 10 μg/mL. Taken together, FACS analysis confirmed that NOTA and 800CW conjugation did not alter the antigen binding affinity or specificity of TRC105.

^{64}Cu-labeling, including final purification using PD-10 columns, took 60 ± 10 min (n = 10). The decay-corrected radiochemical yield was > 85%, based on 25 μg of NOTA-TRC105-800CW or NOTA-cetuximab-800CW per 37 MBq of ^{64}Cu, and the radiochemical purity was > 95%. The specific activity of both ^{64}Cu-NOTA-TRC105-800CW and ^{64}Cu-NOTA-cetuximab-800CW was ~1.3 GBq/mg of protein, assuming complete recovery of the NOTA-mAb-800CW conjugates after size exclusion column chromatography.

BLI to monitor lung tumor burden

Stable transfection of 4T1 cells with firefly luciferase did not cause any observable changes in cell proliferation, tumorigenicity, or migration [21]. About one week after i.v. injection, BLI signal of the fLuc-4T1 cells in mouse lung can be readily detected after i.p. injection of D-luciferin (Figure 1b,c). At about three weeks after tumor inoculation, when the BLI signal was sufficiently strong but before mice showed obvious symptoms (e.g., body weight loss, difficulty in breathing, etc.), mice bearing fLuc-4T1 lung metastasis tumors were used for subsequent PET/NIRF imaging studies. The use of BLI enabled convenient and non-invasive monitoring of the tumor burden in the mouse lungs, which ensured that only mice with appropriate tumor burden were used for dual-modality PET/NIRF imaging of tumor angiogenesis, since small microscopic tumors may not have sufficient angiogenic activity for imaging applications.

In vivo PET imaging and ROI analysis

The time points of 4, 24, and 48 h p.i. were chosen for serial PET scans after intravenous tracer injection based on our previous studies, with the first time point in the initial tumor accumulation phase and the latter two points within a plateau of tumor uptake [16, 27]. Coronal PET images that contain the fLuc-4T1 lung tumors are shown in Figure 2a, and representative PET/CT fused images at 48 h p.i. are shown in Figure 2b,c.

Due to excellent in vivo stability of the ^{64}Cu-NOTA complex, liver uptake of ^{64}Cu-NOTA-TRC105-800CW was significantly lower at 4 h p.i. than that observed for ^{64}Cu-DOTA-TRC105 (which may have certain degree of ^{64}Cu-transchelation, thereby increasing radioactivity accumulation in the liver) in our previous study [27]. Meanwhile, blood pool radioactivity was prominent at early time points (due to long circulation half-life of the antibody) which gradually declined over time. The liver uptake of ^{64}Cu-NOTA-TRC105-800CW was 17.7 ± 1.2, 15.8 ± 2.8, and 14.0 ± 1.8 %ID/g at 4, 24, and 48 h p.i. respectively, whereas the radioactivity in the blood was 27.2 ± 2.4, 16.2 ± 1.0, and 15.6 ± 1.0 %ID/g at 4, 24, and 48 h p.i., respectively (n = 3; Figure 3a). The fLuc-4T1 lung tumor uptake of ^{64}Cu-NOTA-TRC105-800CW was clearly visible as early as 4 h p.i. (Figure 2a) which reached a plateau at around 24 h p.i. (11.9 ± 1.2, 13.9 ± 3.9, and 13.4 ± 2.1 %ID/g at 4, 24, and 48 h p.i. respectively; n = 3; Figure 3a,d).

Administering a blocking dose of TRC105 at 2 h before ^{64}Cu-NOTA-TRC105-800CW injection reduced the tumor uptake to background level ($P < 0.01$ at all time points examined when compared with mice injected with ^{64}Cu-NOTA-TRC105-800CW alone; n = 3; Figure 2a,Figure 3b,3d), which clearly indicated CD105 specificity of the tracer in vivo. Radioactivity in the blood (15.3 ± 1.1, 9.6 ± 1.2, and 6.6 ± 1.1 %ID/g at 4, 24, and 48 h p.i. respectively; n = 3; Figure 3b) was also significantly lower for the “blocking” group. Liver uptake was 20.0 ± 1.7, 14.3 ± 1.1, and 10.3 ± 1.2 %ID/g at 4, 24, and 48 h p.i., respectively (n = 3; Figure 3b), similar as that of mice injected with ^{64}Cu-NOTA-TRC105-800CW alone. Together, these data suggested faster blood clearance of ^{64}Cu-NOTA-TRC105-800CW when most CD105 in the mice was already bound by pre-injected TRC105, thereby leaving no CD105 for the tracer to interact with.

To further investigate CD105 specificity of ^{64}Cu-NOTA-TRC105-800CW, ^{64}Cu-NOTA-cetuximab-800CW was used as an isotype-matched control. Both TRC105 and cetuximab are human/murine chimeric IgG1 mAbs. Since cetuximab does not cross-react with murine tissues, it serves as an excellent control for investigating tracer uptake in the tumor due to passive targeting only (i.e., the enhanced permeability and retention effect). As can be seen in Figure 2a & Figure 3c, the fLuc-4T1 lung tumor uptake of ^{64}Cu-NOTA-cetuximab-800CW (5.4 ± 1.6, 5.0 ± 0.3, and 3.7 ± 1.4 %ID/g at 4, 24, and 48 h p.i., respectively; n = 3; Figure 3c,d) was significantly lower than that of ^{64}Cu-NOTA-TRC105-800CW at all time points examined ($P < 0.01$), which further confirmed CD105 specificity of ^{64}Cu-NOTA-TRC105-800CW in the metastatic lesions in vivo.

The tumor-to-liver ratios derived from ROI analysis of the PET data were 0.67 ± 0.07, 0.87 ± 0.13, and 0.96 ± 0.19 for ^{64}Cu-NOTA-TRC105-800CW, 0.24 ± 0.06, 0.27 ± 0.05, and 0.44 ± 0.21 for ^{64}Cu-NOTA-TRC105-800CW with a blocking dose of TRC105, and 0.23 ± 0.08, 0.30 ± 0.04, and 0.25 ± 0.06 for ^{64}Cu-NOTA-cetuximab-800CW at 4, 24, and 48 h p.i. (n = 3). The tumor-to-muscle ratios were 5.43 ± 2.72, 7.17 ± 1.78, and 7.17 ± 0.98 for ^{64}Cu-NOTA-TRC105-800CW, 4.43 ± 1.20, 3.34 ± 0.70, and 3.88 ± 1.58 for ^{64}Cu-NOTA-TRC105-800CW with a blocking dose of TRC105, 6.39 ± 3.46, 5.00 ± 1.41, and 3.55 ± 0.73 for ^{64}Cu-NOTA-cetuximab-800CW, at 4, 24, and 48 h p.i. (n = 3). Overall, ^{64}Cu-NOTA-TRC105-800CW exhibited significantly better tumor contrast over the two control groups, in addition to higher %ID/g values for fLuc-4T1 lung tumor uptake.

Ex vivo imaging, autoradiography, and biodistribution studies

After the last PET scans at 48 h p.i., mice were euthanized and major organs were subjected for ex vivo BLI/NIRF/PET imaging (Figure 4a). BLI clearly delineated multiple fLuc-4T1 tumor nodules (~1 mm in diameter) in the mouse lung, which confirmed stable expression of firefly luciferase in the fLuc-4T1 cells and corroborated the in vivo BLI findings. Ex vivo NIRF and PET imaging both correlated well with the in vivo PET data, in which the

fLuc-4T1 lung tumor uptake of ^{64}Cu-NOTA-TRC105-800CW was higher than all major organs except the liver (which is responsible for tracer clearance). Similar uptake in normal organs was observed for ^{64}Cu-NOTA-cetuximab-800CW and ^{64}Cu-NOTA-TRC105-800CW in the "blocking" group, however the tumor uptake was significantly lower. Taken together, ex vivo imaging confirmed the in vivo data and validated CD105 specificity of ^{64}Cu-NOTA-TRC105-800CW in vivo.

The high-resolution autoradiography images clearly manifested multiple small metastatic tumor nodules, corroborated by the findings from ex vivo NIRF imaging (Figure 4b). Overall, the distribution of ^{64}Cu (detected by autoradiography) and 800CW (detected by NIRF imaging) matched well, which suggested good in vivo stability of ^{64}Cu-NOTA-TRC105-800CW. Biodistribution studies after ex vivo BLI/NIRF/PET imaging was also in good agreement with the in vivo PET results, where the fLuc-4T1 lung tumors had higher uptake of ^{64}Cu-NOTA-TRC105-800CW than most major organs (Figure 5a). Spleen and kidneys also had prominent uptake of ^{64}Cu-NOTA-TRC105-800CW at 48 h p.i., however the absolute uptake level was significantly lower than that in the fLuc-4T1 lung tumors. On average, the weight difference between the fLuc-4T1 tumor-bearing lung and normal mouse lung was ~0.1g, which correlates to a total tumor volume of ~100 mm^3.

A comparison of the biodistribution data between ^{64}Cu-NOTA-TRC105-800CW and ^{64}Cu-NOTA-cetuximab-800CW at 48 h p.i. revealed that the uptake of ^{64}Cu-NOTA-cetuximab-800CW was similar to ^{64}Cu-NOTA-TRC105-800CW in most organs except the fLuc-4T1 tumor-bearing lung (Figure 5b). When comparing fLuc-4T1 tumor uptake in mice injected with ^{64}Cu-NOTA-TRC105-800CW alone and the "blocking" group, a similar trend was observed (i.e. comparable tracer uptake in most normal tissues but significantly lower uptake in the fLuc-4T1 tumor-bearing lung in the "blocking" group; Figure 5a). Statistical significance was achieved for the fLuc-4T1 tumor-bearing lung for both comparisons ($P < 0.01$; $n = 3$), corroborating the PET findings. Overall, the quantitative data obtained from biodistribution studies and PET scans matched very well, confirming that ROI analysis of non-invasive PET scans truly reflected tracer distribution in vivo.

Linear correlation was carried out between the ex vivo NIRF data (total signal for ROI covering the entire fLuc-4T1 tumor-bearing lungs) and tracer uptake (%ID/g values based on PET scans or biodistribution studies), using a total of 9 data points for each (fLuc-4T1 tumor-bearing lungs at 48 h p.i. for three groups of mice with three mice per group). As evidenced in Figure 4c, statistically significant ($P < 0.01$ in both cases) linear correlation was achieved with R^2 values of 0.80 (ex vivo NIRF vs %ID/g based on biodistribution) and 0.79 (ex vivo NIRF vs %ID/g based on PET scans) respectively, indicating that NIRF imaging can obtain relatively accurate quantitative results in ex vivo settings when compared with PET scans or biodistribution studies based on γ-counting.

Histology

Immunofluorescence CD105/CD31 co-staining of various tissues revealed that CD105 expression in the fLuc-4T1 lung tumors was primarily on the tumor vasculature, as evidenced by good co-localization of CD105 and CD31 staining (Figure 6). Of note, perfect overlap of CD31 and CD105 staining is not expected since CD105 only stains actively proliferating vascular endothelial cells (i.e., a sub population of CD31 positive cells). Normal mouse lung, liver, and spleen all exhibited low level of CD105 staining, indicating that these tissues do not express high level of CD105. Therefore, uptake of ^{64}Cu-NOTA-TRC105-800CW in the liver/spleen was largely unrelated to CD105 binding and likely attributed to non-specific capture by the reticuloendothelial system and hepatic clearance of the tracer.

Discussion

The goal of this study was to develop a dual-labeled CD105-specific agent for both PET and NIRF imaging of BC lung metastasis, which was successfully achieved. The experimental findings revealed that NOTA-TRC105-800CW specifically bound to HUVECs (CD105 positive) but not to MCF-7 cells (CD105 negative) in vitro. In addition, we have demonstrated that ^{64}Cu-NOTA-TRC105-800CW can detect small lung metastatic tumor nodules with high specificity and affinity in vivo and ex vivo. Therefore, this dual-labeled agent can potentially enable non-invasive detection of BC lung metastatic lesions and subsequently assist in surgical removal of tumor nodules with molecular imaging guidance (a proof-of-principle study for image-guided surgery in a subcutaneous 4T1 tumor model in nude mice was shown in Figure 7), through PET and NIRF imaging respectively in future clinical investigation. The incorporation of two imaging labels onto a single agent (e.g., TRC105), if the chemical modification is minimal and does not compromise the antigen binding affinity/specificity, is synergistic and can offer many advantages over single modality imaging. For example, such combination can facilitate future clinical translation of a single agent for both imaging modalities, instead of two different imaging agents, and can therefore significantly reduce the cost in the development of clinically translatable agents.

To minimize the interference with its antigen binding affinity/specificity is one of the key challenges in PET imaging with a radiolabeled antibody. Serendipitously, TRC105 has only one lysine residue within each of the complementarity-determining region (CDR), which has a total of ~1,400 amino acid residues and ~70 lysines in the entire mAb [19]. Therefore, the possibility of NOTA or 800CW conjugation at the lysine residue within the CDR region is very low, which was confirmed by FACS studies (Figure 1a).

For preclinical PET imaging using radiometals, ^{64}Cu is one of the most widely used isotopes for immunoPET and a variety of chelators are commercially available for ^{64}Cu-labeling [28]. One of the requirements for PET imaging with a ^{64}Cu-labeled mAb to accurately represent the in vivo distribution of the mAb is that the tracer should be sufficiently stable throughout the imaging period, since PET scanners only detect the distribution of the radioisotope but not the mAb itself. After constant debate over the last decade, it is now generally recognized that NOTA is one of the most stable chelators for ^{64}Cu-labeling of proteins such as mAbs [29]. ^{64}Cu-NOTA-TRC105-800CW exhibited significantly lower liver uptake and higher blood radioactivity at 4 h p.i. than that of ^{64}Cu-DOTA-TRC105 in our previous study [27], which strongly suggested better in vivo stability of ^{64}Cu-NOTA over ^{64}Cu-DOTA conjugated TRC105, as liver is the major organ for potential transchelation of ^{64}Cu. Since the spatial resolution of PET is relatively low (~ 2 mm), we performed autoradiography of the fLuc-4T1 tumor-bearing lungs to visualize the distribution of ^{64}Cu-NOTA-TRC105-800CW in more detail. The small tumor nodules within the lung, detected by autoradiography and ex vivo NIRF imaging (Figure 4b), co-localized quite well and confirmed the good in vivo stability of the tracer.

^{18}F-FDG PET/CT is commonly used for imaging metastatic lung tumor nodules in clinical patient management [30, 31]. However, ^{18}F-FDG is an agent for imaging glucose metabolism, which is not highly tumor specific and it can also be taken up by inflamed tissues and other benign processes. The visualization of small metastatic lung lesions can be severely interfered by the high uptake of ^{18}F-FDG in the myocardium, especially in preclinical mouse models. One major limitation of PET imaging with radiolabeled intact antibodies is the relatively long circulation half-life [32, 33], which created a similar sub-optimal scenario for detecting lung metastatic tumor nodules as ^{18}F-FDG PET, except that prominent radioactivity is in the blood pool instead of the myocardium. Therefore, extensive ex vivo studies such as PET/NIRF imaging and histology were carried out to confirm the in

vivo PET findings in this work. This limitation can be alleviated in future studies through the use of radiolabeled antibody fragments [34, 35], which can maintain the antigen-binding affinity/specificity of the parent antibodies but have much shorter circulation half-life, hence lower background signal in the heart and blood vessels.

Conclusion

We report the development, characterization, and investigation of a molecular probe ^{64}Cu-NOTA-TRC105-800CW for PET/NIRF imaging of tumor angiogenesis in a mouse model of BC experimental lung metastasis. Rapid, persistent, and CD105-specific uptake of ^{64}Cu-NOTA-TRC105-800CW was observed in the metastatic lung nodules with both PET and NIRF imaging, which was validated by various in vitro, in vivo, and ex vivo experiments. In addition, this agent was also successfully employed for NIRF imaged-guided surgical removal of subcutaneously implanted tumors in mice. Such PET/NIRF agents for imaging of tumor angiogenesis may play multiple roles in metastatic BC patient management upon future clinical translation, such as diagnosis, staging, monitoring the efficacy of therapy, as well as image-guided surgery.

Acknowledgments

This work was supported, in part, by the University of Wisconsin Carbone Cancer Center, the Department of Defense (W81XWH-11-1-0644), and the Elsa U. Pardee Foundation. We thank Dr. Xiaoyuan Chen and Dr. Gang Niu for providing the fLuc-4T1 cells.

References

1. Siegel R, Naishadham D, Jemal A. Cancer statistics, 2012. CA Cancer J Clin. 2012; 62:10–29. [PubMed: 22237781]
2. Eckhardt BL, Francis PA, Parker BS, Anderson RL. Strategies for the discovery and development of therapies for metastatic breast cancer. Nat Rev Drug Discov. 2012; 11:479–497. [PubMed: 22653217]
3. Weigelt B, Peterse JL, van 't Veer LJ. Breast cancer metastasis: markers and models. Nat Rev Cancer. 2005; 5:591–602. [PubMed: 16056258]
4. Gambhir SS, Czernin J, Schwimmer J, Silverman DH, Coleman RE, Phelps ME. A tabulated summary of the FDG PET literature. J Nucl Med. 2001; 42:1S–93S. [PubMed: 11483694]
5. Alauddin MM. Positron emission tomography (PET) imaging with ^{18}F-based radiotracers. Am J Nucl Med Mol Imaging. 2012; 2:55–76. [PubMed: 23133802]
6. Iagaru A. ^{18}F-FDG PET/CT: timing for evaluation of response to therapy remains a clinical challenge. Am J Nucl Med Mol Imaging. 2011; 1:63–64. [PubMed: 23133796]
7. Hanahan D, Weinberg RA. Hallmarks of cancer: the next generation. Cell. 2011; 144:646–674. [PubMed: 21376230]
8. von Elstermann M. Metastasis: Which way to the lungs? Nat Rev Cancer. 2008; 8:410–411.
9. Ikushima H, Miyazono K. TGFbeta signalling: a complex web in cancer progression. Nat Rev Cancer. 2010; 10:415–424. [PubMed: 20495575]
10. Fonsatti E, Nicolay HJ, Altomonte M, Covre A, Maio M. Targeting cancer vasculature via endoglin/CD105: a novel antibody-based diagnostic and therapeutic strategy in solid tumours. Cardiovasc Res. 2010; 86:12–19. [PubMed: 19812043]
11. Dallas NA, Samuel S, Xia L, Fan F, Gray MJ, Lim SJ, et al. Endoglin (CD105): a marker of tumor vasculature and potential target for therapy. Clin Cancer Res. 2008; 14:1931–1937. [PubMed: 18381930]
12. Eary JF, Hawkins DS, Rodler ET, Conrad EU 3rd. ^{18}F-FDG PET in sarcoma treatment response imaging. Am J Nucl Med Mol Imaging. 2011; 1:47–53. [PubMed: 23133794]
13. Grassi I, Nanni C, Allegri V, Morigi JJ, Montini GC, Castellucci P, et al. The clinical use of PET with ^{11}C-acetate. Am J Nucl Med Mol Imaging. 2012; 2:33–47. [PubMed: 23133801]

14. James ML, Gambhir SS. A molecular imaging primer: modalities, imaging agents, and applications. Physiol Rev. 2012; 92:897–965. [PubMed: 22535898]
15. Nolting DD, Nickels ML, Guo N, Pham W. Molecular imaging probe development: a chemistry perspective. Am J Nucl Med Mol Imaging. 2012; 2:273–306. [PubMed: 22943038]
16. Zhang Y, Hong H, Engle JW, Yang Y, Theuer CP, Barnhart TE, et al. Positron emission tomography and optical imaging of tumor CD105 expression with a dual-labeled monoclonal antibody. Mol Pharm. 2012; 9:645–653. [PubMed: 22292418]
17. Hong H, Zhang Y, Severin GW, Yang Y, Engle JW, Niu G, et al. Multimodality Imaging of Breast Cancer Experimental Lung Metastasis with Bioluminescence and a Monoclonal Antibody Dual-Labeled with ^{89}Zr and IRDye 800CW. Mol Pharm. 2012; 9:2339–2349.
18. Zhang Y, Hong H, Severin GW, Engle JW, Yang Y, Goel S, et al. ImmunoPET and near-infrared fluorescence imaging of CD105 expression using a monoclonal antibody dual-labeled with ^{89}Zr and IRDye 800CW. Am J Transl Res. 2012; 4:333–346. [PubMed: 22937210]
19. Seon BK, Haba A, Matsuno F, Takahashi N, Tsujie M, She X, et al. Endoglin-targeted cancer therapy. Curr Drug Deliv. 2011; 8:135–143. [PubMed: 21034418]
20. Rosen LS, Hurwitz HI, Wong MK, Goldman J, Mendelson DS, Figg WD, et al. A phase I first-in-human study of TRC105 (Anti-Endoglin Antibody) in patients with advanced cancer. Clin Cancer Res. 2012; 18:4820–4829. [PubMed: 22767667]
21. Cao Q, Cai W, Niu G, He L, Chen X. Multimodality imaging of IL-18-binding protein-Fc therapy of experimental lung metastasis. Clin Cancer Res. 2008; 14:6137–6145. [PubMed: 18829492]
22. Hong H, Severin GW, Yang Y, Engle JW, Zhang Y, Barnhart TE, et al. Positron emission tomography imaging of CD105 expression with ^{89}Zr-Df-TRC105. Eur J Nucl Med Mol Imaging. 2012; 39:138–148. [PubMed: 21909753]
23. Zhang Y, Hong H, Engle JW, Yang Y, Barnhart TE, Cai W. Positron Emission Tomography and Near-Infrared Fluorescence Imaging of Vascular Endothelial Growth Factor with Dual-Labeled Bevacizumab. Am J Nucl Med Mol Imaging. 2012; 2:1–13. [PubMed: 22229128]
24. Hong H, Benink HA, Zhang Y, Yang Y, Uyeda HT, Engle JW, et al. HaloTag: a novel reporter gene for positron emission tomography. Am J Transl Res. 2011; 3:392–403. [PubMed: 21904659]
25. Cai W, Wu Y, Chen K, Cao Q, Tice DA, Chen X. *In vitro* and *in vivo* characterization of ^{64}Cu-labeled Abegrin™, a humanized monoclonal antibody against integrin $\alpha_v\beta_3$. Cancer Res. 2006; 66:9673–9681. [PubMed: 17018625]
26. Hong H, Zhang Y, Engle JW, Nayak TR, Theuer CP, Nickles RJ, et al. In vivo targeting and positron emission tomography imaging of tumor vasculature with ^{66}Ga-labeled nano-graphene. Biomaterials. 2012; 33:4147–4156. [PubMed: 22386918]
27. Hong H, Yang Y, Zhang Y, Engle JW, Barnhart TE, Nickles RJ, et al. Positron emission tomography imaging of CD105 expression during tumor angiogenesis. Eur J Nucl Med Mol Imaging. 2011; 38:1335–1343. [PubMed: 21373764]
28. Wadas TJ, Wong EH, Weisman GR, Anderson CJ. Coordinating radiometals of copper, gallium, indium, yttrium, and zirconium for PET and SPECT imaging of disease. Chem Rev. 2010; 110:2858–2902. [PubMed: 20415480]
29. Dearling JL, Voss SD, Dunning P, Snay E, Fahey F, Smith SV, et al. Imaging cancer using PET--the effect of the bifunctional chelator on the biodistribution of a ^{64}Cu-labeled antibody. Nucl Med Biol. 2011; 38:29–38. [PubMed: 21220127]
30. Geus-Oei LF, Oyen WJ. Predictive and prognostic value of FDG-PET. Cancer Imaging. 2008; 8:70–80. [PubMed: 18390390]
31. Iagaru A, Masamed R, Keesara S, Conti PS. Breast MRI and ^{18}F FDG PET/CT in the management of breast cancer. Ann Nucl Med. 2007; 21:33–38. [PubMed: 17373334]
32. van Dongen GA, Vosjan MJ. Immuno-positron emission tomography: shedding light on clinical antibody therapy. Cancer Biother Radiopharm. 2010; 25:375–385. [PubMed: 20707716]
33. Wu AM. Antibodies and antimatter: the resurgence of immuno-PET. J Nucl Med. 2009; 50:2–5. [PubMed: 19091888]
34. Zhang Y, Hong H, Orbay H, Valdovinos HF, Nayak TR, Theuer CP, et al. PET imaging of CD105/endoglin expression with a $^{61/64}$Cu-labeled Fab antibody fragment. Eur J Nucl Med Mol Imaging. 2013 ePub.

35. Hong H, Zhang Y, Orbay H, Valdovinos HF, Nayak TR, Bean J, et al. Positron Emission Tomography Imaging of Tumor Angiogenesis with a $^{61/64}$Cu-Labeled F(ab')$_2$ Antibody Fragment. Mol Pharm. 2013 ePub.

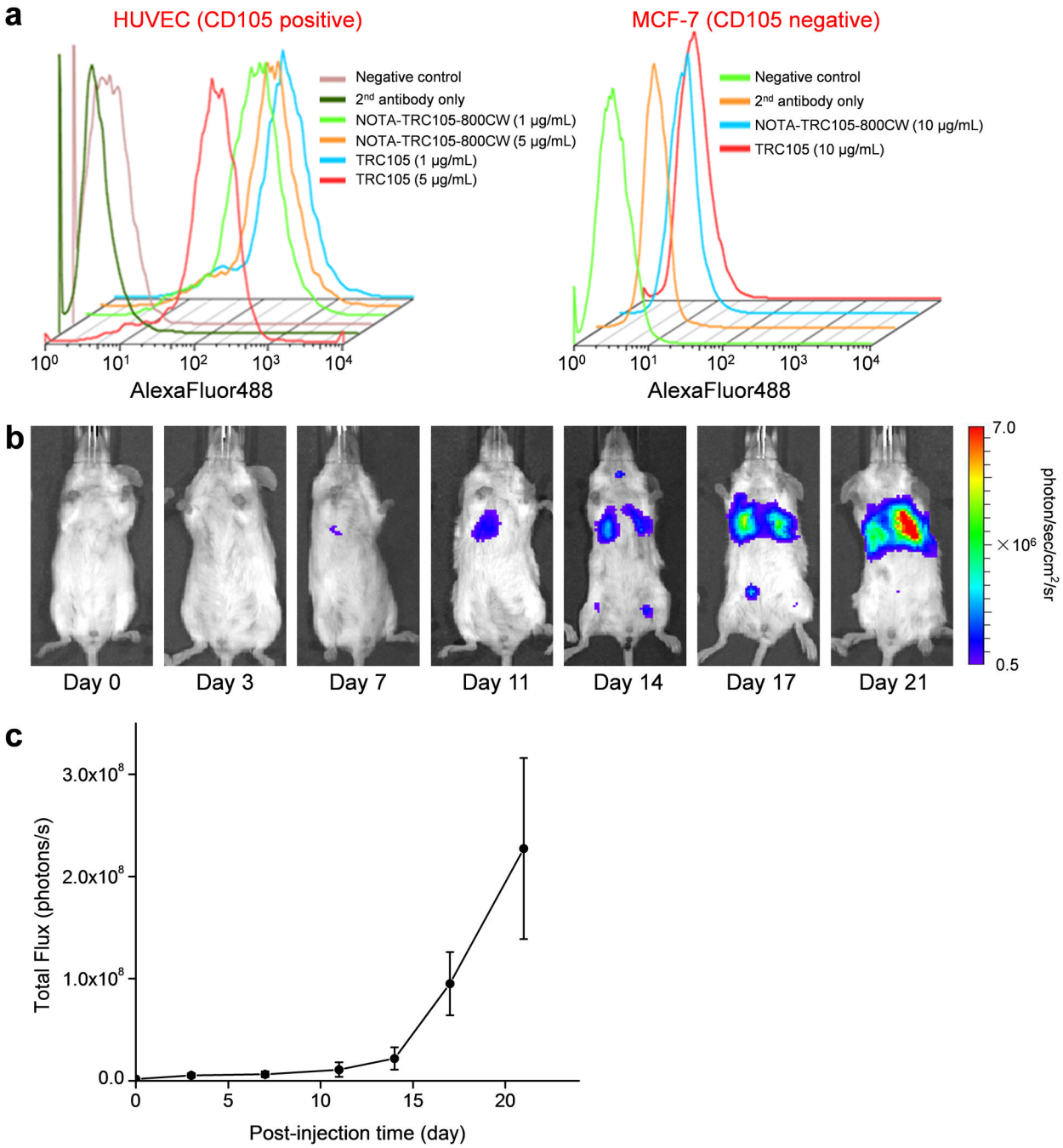

Figure 1.

In vitro characterization of NOTA-TRC105-800CW and monitoring of fLuc-4T1 lung tumor burden with bioluminescence imaging. **a** Flow cytometry analysis of TRC105 and NOTA-TRC105-800CW in HUVECs (CD105 positive) and MCF-7 human breast cancer cells (CD105 negative) at multiple concentrations. Data from various control experiments are also shown. **b** Representative serial bioluminescence images of fLuc-4T1 lung tumor-bearing mice after intravenous injection of fLuc-4T1 cells. **c** Total photon flux of the bioluminescence signal (representing the total tumor burden) from the mouse lung (n = 8).

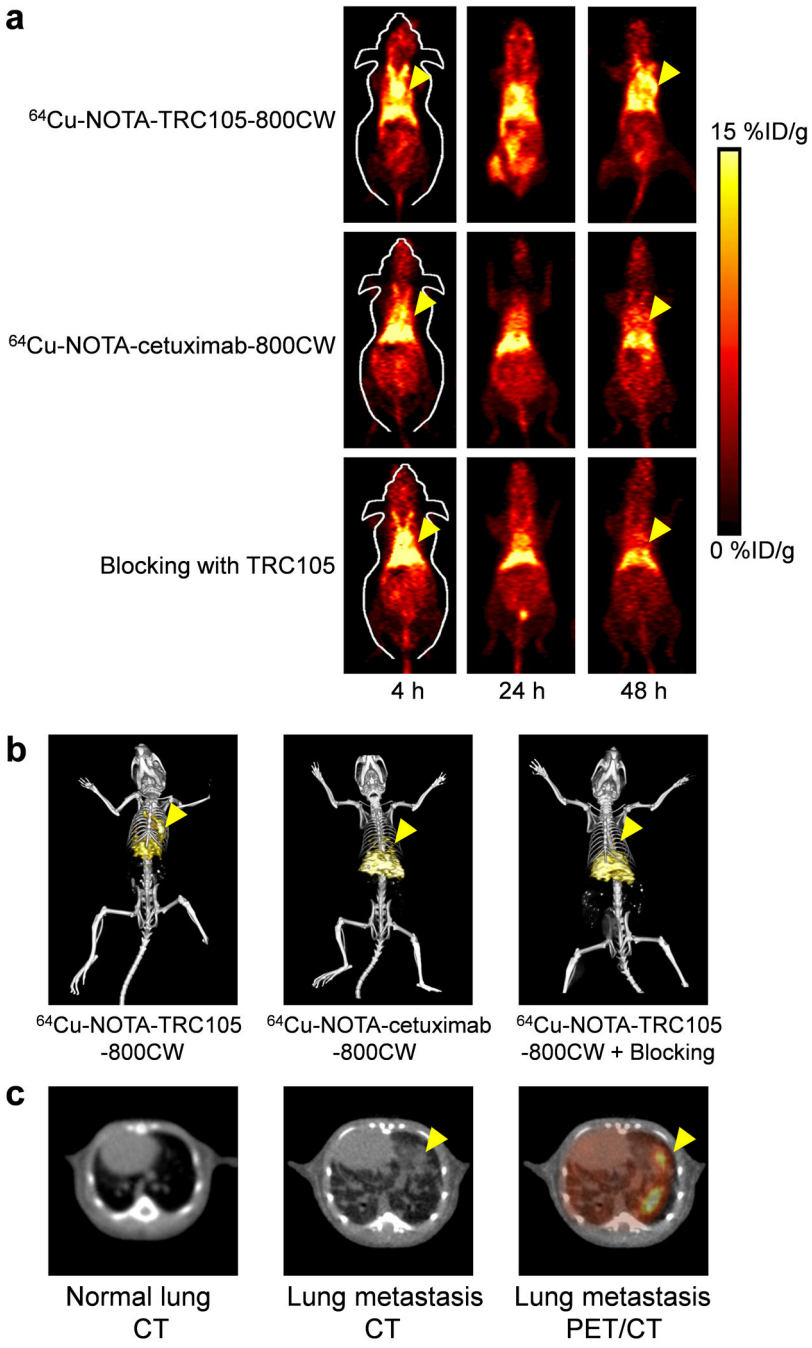

Figure 2.

Serial in vivo PET/CT imaging of fLuc-4T1 lung tumor-bearing mice. **a** Serial coronal PET images at 4, 24, and 48 h post-injection of ^{64}Cu-NOTA-TRC105-800CW, ^{64}Cu-NOTA-cetuximab-800CW, or ^{64}Cu-NOTA-TRC105-800CW after a 2 mg pre-injected dose of TRC105 (i.e., blocking). **b** Representative PET/CT images of fLuc-4T1 tumor-bearing mice in the three groups at 48 h post-injection. **c** Representative CT images of normal mouse lung, fLuc-4T1 lung metastasis, and a PET/CT fused image at 48 h post-injection of ^{64}Cu-NOTA-TRC105-800CW into fLuc-4T1 lung tumor-bearing mice. Arrowheads indicate the fLuc-4T1 tumors.

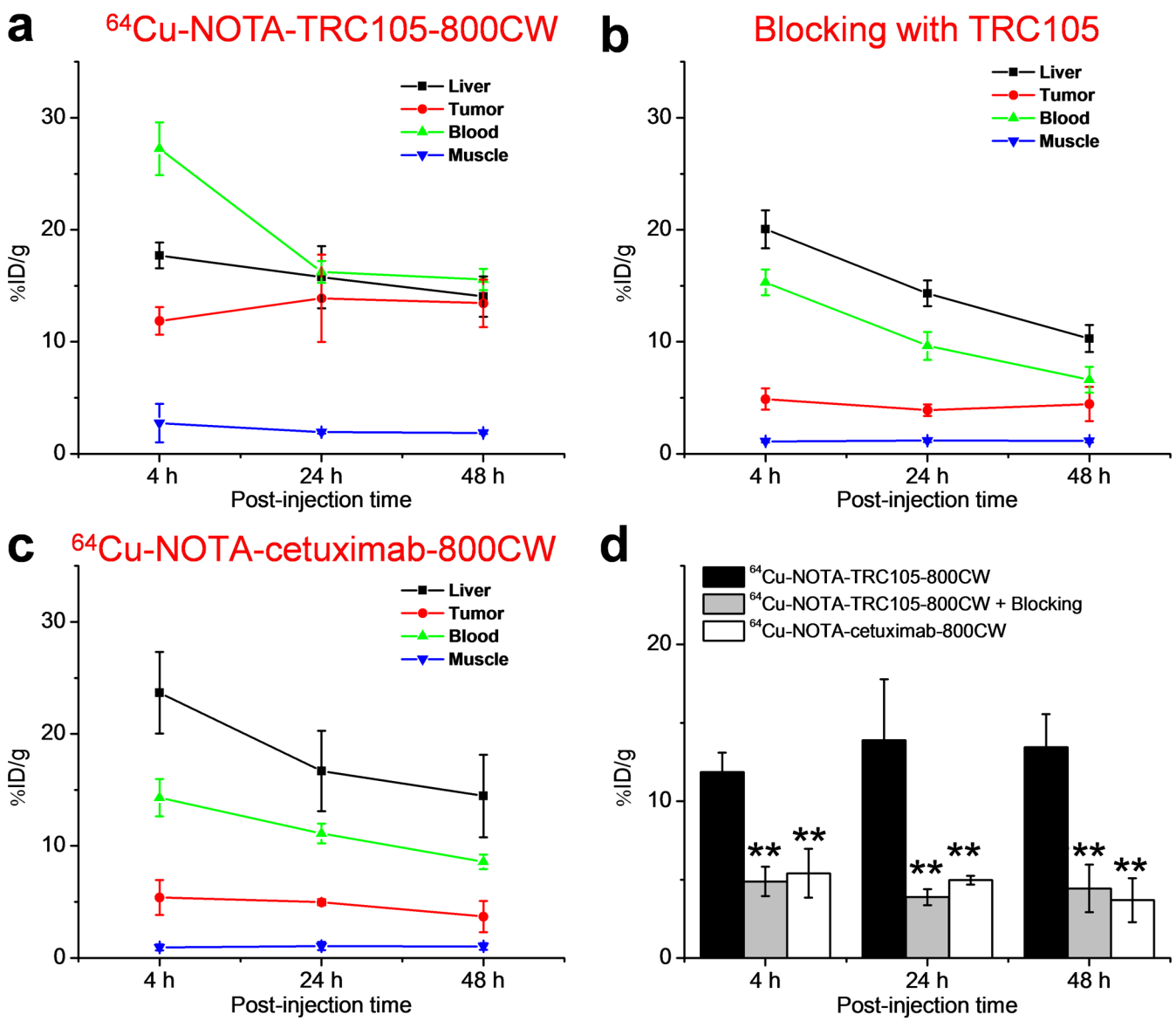

Figure 3.

Quantitative analysis of the PET data. **a** Time-activity curves of the liver, fLuc-4T1 lung tumor, blood, and muscle upon intravenous injection of ^{64}Cu-NOTA-TRC105-800CW. **b** Time-activity curves of the liver, fLuc-4T1 lung tumor, blood, and muscle upon intravenous injection of ^{64}Cu-NOTA-TRC105-800CW, after a blocking dose of 2 mg of TRC105. **c** Time-activity curves of the liver, fLuc-4T1 lung tumor, blood, and muscle upon intravenous injection of ^{64}Cu-NOTA-cetuximab-800CW. **d** Comparison of the fLuc-4T1 lung tumor uptake in the three groups. n = 3; **: $P < 0.01$.

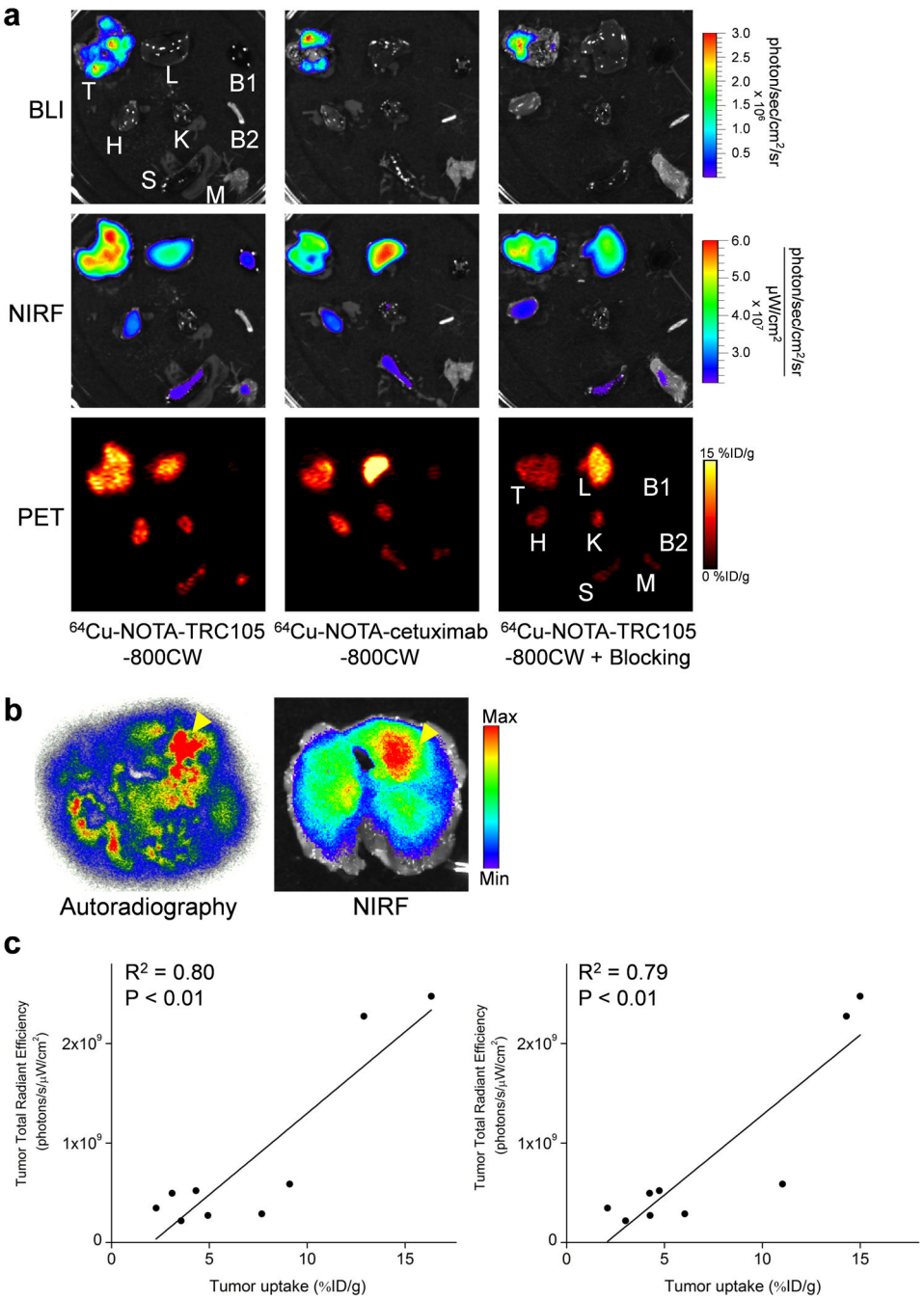

Figure 4.

Ex vivo imaging at 48 h post-injection of each tracer and correlation analysis. **a** Ex vivo bioluminescence imaging (BLI), near-infrared fluorescence (NIRF), and positron emission tomography (PET) imaging of major organs at 48 h post-injection of each tracer. Images are representative of 3 mice per group. T: fLuc-4T1 tumor-bearing lung, L: liver, B1: blood, H: heart, K: kidney, B2: bone, S: spleen, M: muscle. **b** Representative autoradiography and corresponding NIRF images of the entire fLuc-4T1 tumor-bearing lung tissue at 48 h post-injection of ^{64}Cu-NOTA-TRC105-800CW. Arrowheads indicate tumor nodules. **c** Linear correlation of the total ex vivo NIRF signal, in all nine fLuc-4T1 tumor-bearing lung at 48 h

post-injection, with the %ID/g values obtained from biodistribution studies (left) or analysis of the PET data (right).

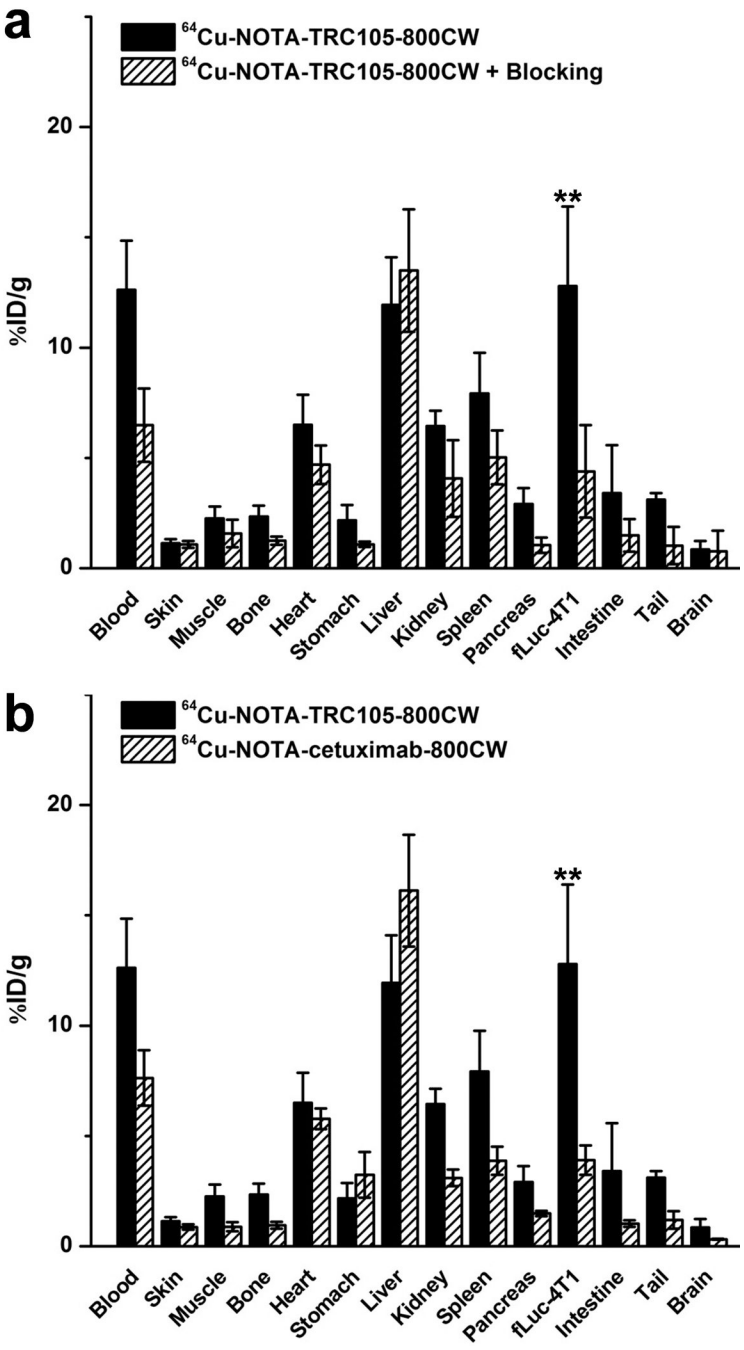

Figure 5.

a Biodistribution in fLuc-4T1 lung tumor-bearing mice at 48 h post-injection of ^{64}Cu-NOTA-TRC105-800CW or ^{64}Cu-NOTA-TRC105-800CW after a blocking dose of TRC105. **b** Biodistribution in fLuc-4T1 lung tumor-bearing mice at 48 h post-injection of ^{64}Cu-NOTA-TRC105-800CW or ^{64}Cu-NOTA-cetuximab-800CW. **: $P < 0.01$. $n = 3$.

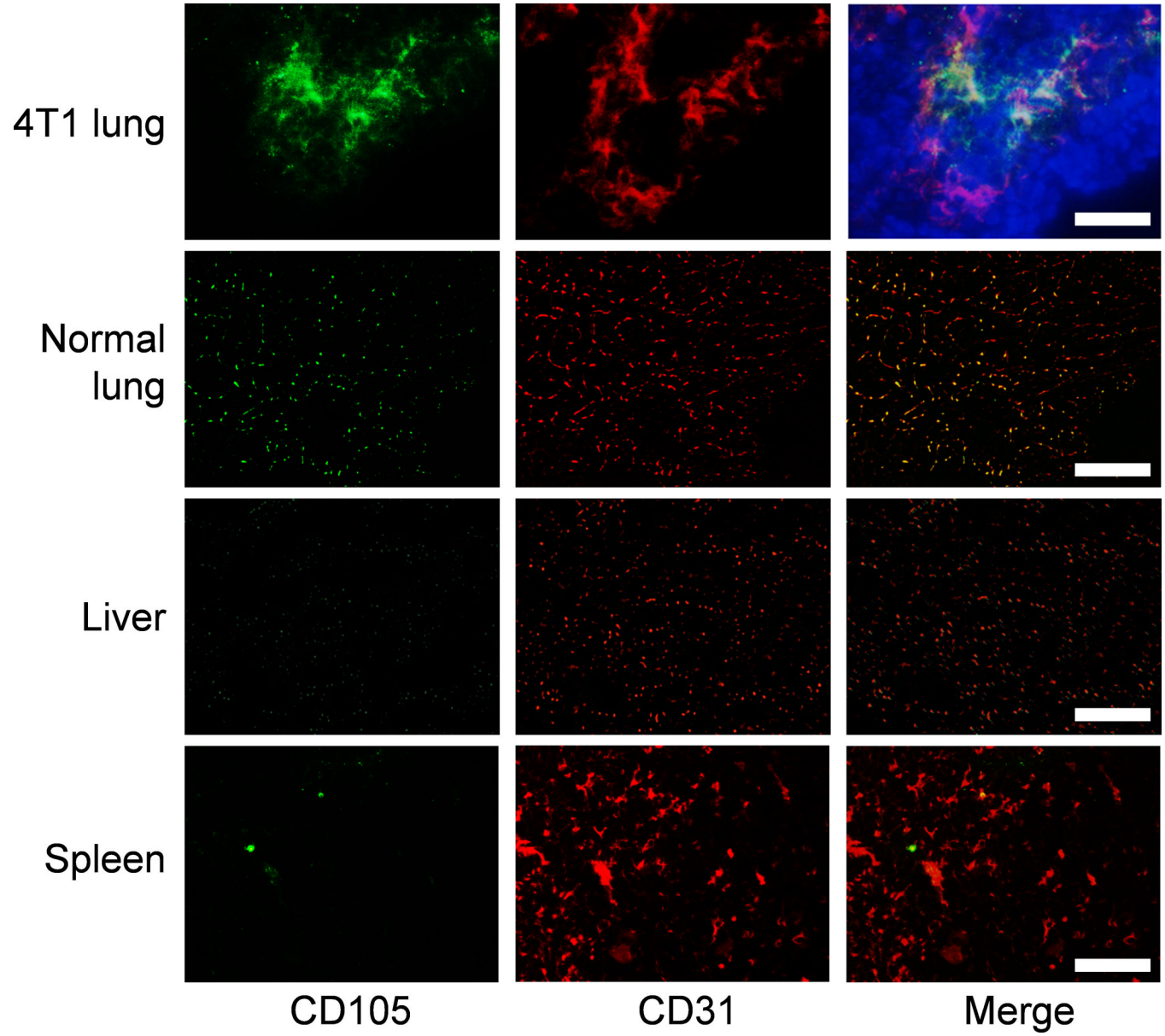

Figure 6.
Immunofluorescence staining of the fLuc-4T1 tumor lung, normal mouse lung, liver, and spleen tissue sections. Green: CD105; red: CD31; blue: DAPI. All images were acquired under the same conditions and displayed at the same scale. Magnification: 200×. Scale bar: 50 μm.

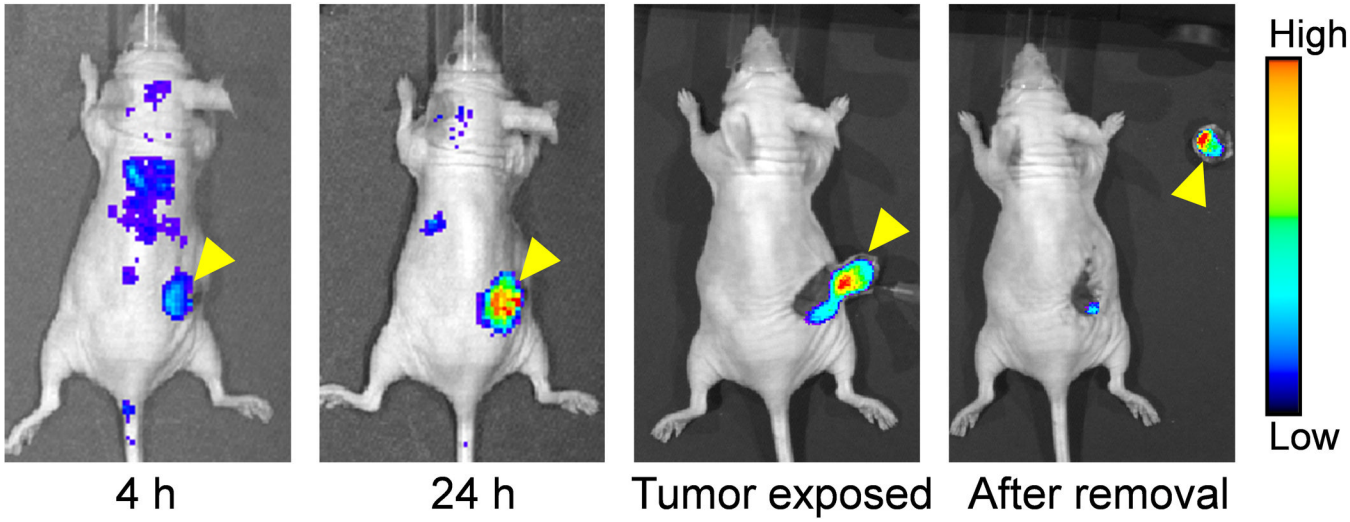

Figure 7.
Near-infrared fluorescence image-guided surgical removal of subcutaneous 4T1 tumors in nude mice, after intravenous injection of NOTA-TRC105-800CW. Mice were subjected to optical imaging at 4 and 24 h post-injection, immediately after the skin was open and tumor exposed, and after surgical removal of the tumor. Arrowheads indicate the 4T1 tumors in all cases.